


Interface involved Dresselhaus spin-orbit coupling in GaInAs/AlInAs heterostructures

Hao Yang,¹ Qingxuan Wang,¹ and Jiyong Fu^{1,2,*}

¹*Department of Physics, Qufu Normal University, 273165 Qufu, Shandong, China*

²*Instituto de Física, Universidade de Brasília, Brasília 70919-970, Distrito Federal, Brazil*

 (Received 16 April 2021; revised 31 August 2021; accepted 2 September 2021; published 20 September 2021)

The interfacial effect in nanosystems is crucial for diverse fields of physics. Here we explore in detail the interface associated Dresselhaus spin-orbit (SO) coupling, which comprises the *usual* linear $\beta_{v,u}$ (Γ_u) and cubic $\beta_{v,3}$ (Γ_3) contributions as well as the *interface*-induced term $\beta_{v,int}$ (Γ_{int}) of intrasubband (intersubband) kinds. Focusing on ordinary $\text{Al}_{0.48}\text{In}_{0.52}\text{As}/\text{Ga}_{0.47}\text{In}_{0.53}\text{As}$ heterostructures with either one or two occupied subbands, we perform a self-consistent Poisson-Schrödinger calculation to determine all the relevant SO contributions. We observe that the interface SO term becomes intensifying for heterostructures with either a weaker bulk Dresselhaus strength of the barrier layer or a lower interface smoothness. Remarkably, it is found that the renormalized linear Dresselhaus coefficient, which accounts for the interfacial contribution, may change sign as the interface smoothness varies, opening up the feasibility of the interface-engineered topological matter of persistent skyrmion lattice [J. Y. Fu, P. H. Penteado, M. O. Hachiya, D. Loss, and J. C. Egues, *Phys. Rev. Lett.* **117**, 226401 (2016)]. Moreover, we also determine the intersubband Dresselhaus contributions including an emergent *quadratic* term (Γ_2) depending on the interfacial effect and the parity of wave functions. As opposed to intersubband terms of the usual linear (Γ_u) and cubic (Γ_3) kinds, the quadratic contribution leads to unusual avoided crossings of the band dispersion and thus may hybridize spin textures of distinct spin branches. Our results should stimulate experiments probing interface-mediated intra- and intersubband Dresselhaus SO effects and provide an extra leverage for extracting reliable bulk Dresselhaus SO parameters.

DOI: [10.1103/PhysRevB.104.125426](https://doi.org/10.1103/PhysRevB.104.125426)

I. INTRODUCTION

The spin-orbit (SO) interaction coupling an electron spin and its orbital motion acts on moving electrons as an effective magnetic field, enabling the manipulation of spin states through electrical means [1,2]. This essential idea has inspired various proposals on spintronic devices, e.g., spin-field [3–5] and spin Hall effect [6,7] transistors. Recently, SO effects are attracting new twists of interest thanks to emerging new fields of condensed matter, including novel spin textures [8,9], topological insulators [10], Majorana fermions [11,12], and Weyl semimetals [13]. Our recent proposals of the persistent skyrmion lattice [14], stretchable spin helix [15], spin-helix symmetry breaking [16], and opposite SO control [17] also indicate the important role of SO effects in semiconductor nanostructures.

Semiconductors such as GaAs, InAs, and InSb offer various strengths of SO couplings [15,18–21] and are thus suitable for a broad range of spintronic applications, making this subject extraordinarily profound. Very recently, we explored in detail SO properties of wide-gap (e.g., GaN) semiconductors in the wurtzite phase and arrived at a general effective Hamiltonian for electrons, valid for quantum wells, wires, and dots with variously defined geometries and external magnetic fields; Kammermeier *et al.* demonstrated persistent spin textures and currents in SO-coupled wurtzite nanowire-based quantum structures [22], further extending this field [23].

In semiconductor nanostructures, the SO effects usually have two dominant contributions, the Rashba [24] and Dresselhaus [25] terms, arising from the breaking of the structural and crystal inversion symmetries, respectively. For such quantum systems, the interfacial effect, though in general challenging, is crucial for various subjects of physics, e.g., interface-based SO control [26], interface-generated SO torque [27], and spin current [28], as well as interface-induced topological insulator transition [29], magnetic anisotropy [30,31], and Dzyaloshinskii-Moriya interaction [31,32]. Regarding the Rashba SO coupling, the interfacial (structural) contribution alongside contributions from external gates, ionized dopants, and confined electrons has been explored extensively in heterostructures with either one [15,33,34] or two [21,23,35] occupied electron subbands. Also, in single-crystal Fe/GaAs (001) heterostructures, the electric field in a Schottky barrier was found capable of modifying interfacial SO fields [36]. As for the Dresselhaus SO coupling, Dyakonov and Kachorovskii in their seminal work [37] determined the Dresselhaus field for two-dimensional (2D) electrons and the induced spin relaxation. With the help of an $sp^3d^5s^*$ model containing ten atomic orbitals, Alekseev and Nestoklon explored the Dresselhaus SO properties in GaAs quantum wells with only one occupied subband for the s conduction band [38]. However, despite substantial efforts, most studies were mainly restricted to heterostructures of single occupancy (i.e., no interband terms) and of abrupt interfaces [15,34,38–40], and a detailed exploration of the interface-involved Dresselhaus SO terms of both the intra- and intersubband contributions is still not available.

*yongjf@qfnu.edu.cn

Here, starting from the bulk crystal, we adopt the symmetrization procedure for noncommuting operators to take into account the interfacial effect in heterostructures [39,41] and establish a systematic formulation for the interface-mediated Dresselhaus SO coupling. In addition to the *usual* linear $\beta_{v,u}$ (Γ_u) and cubic $\beta_{v,3}$ (Γ_3) contributions, we also obtain the interfacial contribution $\beta_{v,int}$ (Γ_{int}), of intrasubband (intersubband) kinds. Remarkably, we reveal an emergent *quadratic* intersubband term (Γ_2), depending on the interfacial effect and the parity of wave functions. We then consider ordinary $\text{Al}_{0.48}\text{In}_{0.52}\text{As}/\text{Ga}_{0.47}\text{In}_{0.53}\text{As}$ both single and double heterostructures, involving the electron occupancy of either one or two subbands, to determine intra- and intersubband SO properties. The $\text{AlInAs}/\text{GaInAs}$ heterostructures have the stronger SO strength and a larger conduction-band offset than GaAs-based ones [15,21], acting as an ideal candidate of harnessing interfacial SO effects for spintronic applications. We further perform a self-consistent Poisson-Schrödinger calculation to quantify all the relevant intrasubband (intersubband) Dresselhaus SO contributions. Our results should stimulate experiments probing the interface-mediated intra- and intersubband Dresselhaus SO effects, and provide an extra leverage for extracting a reliable bulk Dresselhaus SO parameter, the value of which is usually controversial in both theory and experiment [39,42].

The rest of this paper is organized as follows. In Sec. II, by accounting for the interfacial effect, we transform the bulk Dresselhaus SO Hamiltonian to a three-dimensional (3D) form for heterostructures grown along the $z||[100]$ direction. Then, we derive the effective 2D form from the corresponding 3D Hamiltonian, and show expressions of the interface-mediated Dresselhaus SO terms of both intra- and intersubband kinds. In Sec. III, we first introduce our system and relevant physical parameters adopted, and further present our self-consistent results and discussion. We summarize our main findings in Sec. IV.

II. MODEL HAMILTONIANS: FROM THREE TO TWO DIMENSIONS

In this section, we first present the Dresselhaus SO term in the bulk case. Then, following the symmetrization procedure for noncommuting operators [39,41], we account for the interfacial effect and generalize the bulk form to that for 2D heterostructures. For generality, we consider two occupied electron subbands, for which both the intra- and intersubband Dresselhaus SO terms including relevant interfacial contributions are derived.

A. Bulk Dresselhaus SO coupling

The Dresselhaus SO coupling, which arises from broken bulk inversion symmetry, in semiconductors with zinc blende structure reads [25]

$$\mathcal{H}_D^{\text{bulk}} = \gamma [\sigma_x k_x (k_y^2 - k_z^2) + \sigma_y k_y (k_z^2 - k_x^2) + \sigma_z k_z (k_x^2 - k_y^2)], \quad (1)$$

with $k_{x,y,z}$ the wave-vector components along the $x||[100]$, $y||[010]$, and $z||[001]$ directions, respectively, and $\sigma_{x,y,z}$ the Pauli matrices. The bulk Dresselhaus SO constant (γ), from

a 14-band $\mathbf{k} \cdot \mathbf{p}$ calculation, is written as $\gamma = \gamma^{(0)} + \gamma^{(1)}$ [42,43], with

$$\gamma^{(0)} = \frac{4}{3} P Q P' \frac{(E_g + \Delta)(E'_g + \Delta') - E_g E'_g}{E_g(E_g + \Delta)E'_g(E'_g + \Delta')} \quad (2)$$

and

$$\gamma^{(1)} = -\frac{4}{9} \Delta^- Q \frac{P^2(3E'_g + 2\Delta') - P'^2(3E_g + 2E'_g + \Delta)}{E_g(E_g + \Delta)E'_g(E'_g + \Delta')}, \quad (3)$$

where P is the interband Kane matrix element, E_g is the fundamental band gap, and Δ is the split-off gap. The corresponding counterparts for the \mathbf{p} conduction band are denoted by P' , E'_g , and Δ' . The parameters Q and Δ^- are associated with interband matrix elements between the \mathbf{p} -conduction and \mathbf{p} -valence bands.

B. Dresselhaus Hamiltonian in heterostructures

Here we show the 3D form of the Dresselhaus SO Hamiltonian for electrons in heterostructures incorporating the impact of interfacial effect. Then, we present the effective 2D expression in the case of two subbands, involving the Dresselhaus SO terms of both intra- and intersubband types. This is beyond available reports in the literature [15,34,38–40], including the seminal work by Dyakonov and Kachorovskii [37], in which 2D electrons with only one occupied subband (i.e., no intersubband terms) were considered and the interfacial effect was ignored.

1. 3D form

We consider quantum heterostructures grown along the $z||[001]$ direction. The corresponding 3D Hamiltonian for electrons including the Dresselhaus SO coupling reads

$$\mathcal{H}^{3D} = \frac{\hbar^2 k^2}{2m^*} - \frac{\hbar^2}{2m^*} \frac{\partial^2}{\partial z^2} + V(z) + \mathcal{H}_D^{3D}, \quad (4)$$

where m^* is the electron effective mass and $k = \sqrt{k_x^2 + k_y^2}$ is the in-plane electron momentum. The third term, $V = V_w + V_g + V_d + V_e$, is the electron confining potential, which is determined self-consistently within the Poisson-Schrödinger Hartree approximation, with V_w the structural potential (band offset), V_g the external gate potential, V_d the doping potential, and V_e the electron Hartree potential. The last term, \mathcal{H}_D^{3D} , describes the Dresselhaus SO interaction in heterostructures. In the literature, this term is often treated in a way of setting the bulk Dresselhaus parameter γ as a common constant shared by distinct layers of heterostructures. Here, to take into account the interfacial effect, γ is considered layer (i.e., z) dependent [39]. Based on the bulk expression [Eq. (1)], one obtains in heterostructures the Dresselhaus term (\mathcal{H}_D^{3D}), which comprises the linear [$\mathcal{H}_D^{3D}(1)$], quadratic [$\mathcal{H}_D^{3D}(2)$], as well as a cubic contribution [$\mathcal{H}_D^{3D}(3)$], i.e., $\mathcal{H}_D^{3D} = \mathcal{H}_D^{3D}(1) + \mathcal{H}_D^{3D}(2) + \mathcal{H}_D^{3D}(3)$, with

$$\mathcal{H}_D^{3D}(1) = k_z \gamma(z) k_z (\sigma_y k_y - \sigma_x k_x), \quad (5)$$

$$\mathcal{H}_D^{3D}(2) = \frac{1}{2} [\gamma(z) k_z + k_z \gamma(z)] \sigma_z (k_x^2 - k_y^2), \quad (6)$$

and

$$\mathcal{H}_D^{3D}{}_{(3)} = \gamma(z)k_x k_y (\sigma_x k_y - \sigma_y k_x), \quad (7)$$

where $k_z = -i\partial_z$. In Eqs. (5) and (6), the *symmetrization* procedure is performed [39,41] since the operator k_z does not commute with $\gamma(z)$. Clearly, when γ is constant throughout the whole heterostructure, $\mathcal{H}_D^{3D}{}_{(1)}$ and $\mathcal{H}_D^{3D}{}_{(3)}$ become the ordinary linear and cubic terms, respectively, i.e., $\mathcal{H}_D^{3D}{}_{(1)} \rightarrow \gamma k_z^2 (\sigma_y k_y - \sigma_x k_x)$ and $\mathcal{H}_D^{3D}{}_{(3)} \rightarrow \gamma k_x k_y (\sigma_x k_y - \sigma_y k_x)$, and the quadratic contribution $\mathcal{H}_D^{3D}{}_{(2)}$ turns to $\gamma k_z \sigma_z (k_x^2 - k_y^2)$.

2. Effective 2D form

Now we are ready to define an effective 2D model from the 3D Hamiltonian [Eq. (4)]. We first self-consistently

$$\mathcal{H}^{2D} = \begin{pmatrix} \varepsilon_{\mathbf{k}1} \mathbb{1} + \beta_{1,\text{eff}} k (\sigma_y \sin \theta - \sigma_x \cos \theta) & \Gamma_{\text{eff}} k (\sigma_y \sin \theta - \sigma_x \cos \theta) \\ -\beta_{1,3} k (\sigma_y \sin 3\theta + \sigma_x \cos 3\theta) & -\Gamma_3 k (\sigma_y \sin 3\theta + \sigma_x \cos 3\theta) + \Gamma_2 k^2 \sigma_z \cos 2\theta \\ \Gamma_{\text{eff}} k (\sigma_y \sin \theta - \sigma_x \cos \theta) & \varepsilon_{\mathbf{k}2} \mathbb{1} + \beta_{1,\text{eff}} k (\sigma_y \sin \theta - \sigma_x \cos \theta) \\ -\Gamma_3 k (\sigma_y \sin 3\theta + \sigma_x \cos 3\theta) + \Gamma_2 k^2 \sigma_z \cos 2\theta & -\beta_{1,3} k (\sigma_y \sin 3\theta + \sigma_x \cos 3\theta) \end{pmatrix}, \quad (8)$$

with θ the angle between \mathbf{k} and the x axis and $\mathbb{1}$ the 2×2 identity matrix. Below we define the Dresselhaus SO coefficients of both intra- and intersubband terms appearing in Eq. (8). Note that the quadratic intersubband term Γ_2 itself is complex as a result of the Hamiltonian remaining invariant under the symmetry operation of the time-reversal operator.

C. Dresselhaus coefficients

For heterostructures with two occupied electron subbands, the projection procedure leading to Eq. (8) amounts to calculating the matrix elements of \mathcal{H}^{3D} [Eq. (4)] in the truncated basis set $\{|\mathbf{k}\nu\sigma\rangle\}$. In this process, we obtain the Dresselhaus SO coefficients of both intrasubband (β) and intersubband (Γ) terms. For the intrasubband SO coupling, since the usual linear term and the interface term have the same functional form, we can group them together with the first-harmonic contribution $\beta_{v,3}$ [44] into a single renormalized term by defining $\beta_{v,\text{eff}} = \beta_{v,u} + \beta_{v,\text{int}} - \beta_{v,3}$, with $\beta_{v,u}$ the usual linear term, $\beta_{v,\text{int}}$ the interface term, and $\beta_{v,3}$ the cubic term,

$$\beta_{v,u} = -\langle \nu | \gamma(z) \partial_z^2 | \nu \rangle, \quad (9)$$

$$\beta_{v,\text{int}} = -\langle \nu | \gamma_{\text{int}}(z) \partial_z | \nu \rangle, \quad (10)$$

and

$$\beta_{v,3} = \langle \nu | \gamma(z) | \nu \rangle k_F^2 / 4. \quad (11)$$

with k_F the Fermi wave vector.

Similarly, for the intersubband terms, we also have the renormalized Dresselhaus SO coefficient $\Gamma_{\text{eff}} = \Gamma_u + \Gamma_{\text{int}} - \Gamma_3$, where Γ_u , Γ_{int} , and Γ_3 denote the usual linear contribution, interface contribution, and cubic contribution, respectively:

$$\Gamma_u = -\langle 1 | \gamma(z) \partial_z^2 | 2 \rangle, \quad (12)$$

$$\Gamma_{\text{int}} = -\langle 1 | \gamma_{\text{int}}(z) \partial_z | 2 \rangle, \quad (13)$$

determine the spin-degenerate eigenvalues $\varepsilon_{\mathbf{k}\nu} = \mathcal{E}_\nu + \hbar^2 k^2 / 2m^*$ and the corresponding eigenspinors $|\mathbf{k}\nu\sigma\rangle = |\mathbf{k}\nu\rangle \otimes |\sigma\rangle$, $\langle \mathbf{r} | \mathbf{k}\nu \rangle = \exp(i\mathbf{k} \cdot \mathbf{r}) \psi_\nu(z)$, of heterostructures in the absence of SO interaction. To more accurately describe the interfacial effect, we solve in our self-consistent procedure the Ben Daniel–Duke model [17,41], which takes into account layer-dependent effective mass, for the spin-degenerate eigensolutions. Here we have defined \mathcal{E}_ν (ψ_ν), $\nu = 1, 2$, as the ν th quantized energy level (wave function) and $\sigma = \uparrow, \downarrow$ as the electron spin component along the z direction.

By projecting the 3D Hamiltonian onto the basis set $\{|\mathbf{k}\nu\sigma\rangle\}$, we obtain an effective 2D model for the Dresselhaus SO coupling in heterostructures with two occupied electron subbands having both intra- and intersubband terms. Then, in the coordinate system $[x||100]$, $[y||010]$ under the basis set $\{|\mathbf{k}1 \uparrow\rangle, |\mathbf{k}1 \downarrow\rangle, |\mathbf{k}2 \uparrow\rangle, |\mathbf{k}2 \downarrow\rangle\}$, our effective 2D model reads

and

$$\Gamma_3 = \langle 1 | \gamma(z) | 2 \rangle k_F^2 / 4. \quad (14)$$

Clearly, in the absence of the interfacial effect with γ being z independent, Γ_{int} and Γ_3 identically vanish [14] due to the orthogonality relation of wave functions of distinct subbands. Furthermore, the interfacial effect also gives rise to a *quadratic* contribution (Γ_2) to intersubband terms, with

$$\Gamma_2 = -\frac{1}{2} i \langle 1 | \gamma(z) \partial_z + \partial_z \gamma(z) | 2 \rangle. \quad (15)$$

Note that the intrasubband quadratic Dresselhaus contribution arising from the interfacial effect is negligibly small primarily because of wave-function parities. In addition, it is also worth noting that the expectation values of k_z^2 and other related operators *implicitly* depend on the gate potential V_g , and also on the doping potential V_d , electron Hartree potential V_e , and structural potential V_w . In our calculation, for each value of V_g , we *self-consistently* determine the total confining potential $V = V_g + V_d + V_e + V_w$ [Eq. (4)] and the eigenstates of the system and further the expectation value of the relevant operators [see Eqs. (9)–(15)].

III. RESULTS AND DISCUSSION

We first introduce our system and relevant parameters adopted. Then, we show our self-consistent calculations of the interface-mediated Dresselhaus SO couplings including both intra- and intersubband terms in a single heterostructure (SH) with either one or two occupied electron subbands. We also compare with the case of a double-heterostructure (DH) configuration, i.e., an ordinary quantum well, which involves the interplay of two heterojunctions and allows for considering a gate-controlled geometry of the well having *local* structural inversion symmetry even under asymmetric doping conditions. Furthermore, emergent unusual avoided crossings of the energy dispersion within the pure Dresselhaus model induced by the quadratic intersubband term, which depends

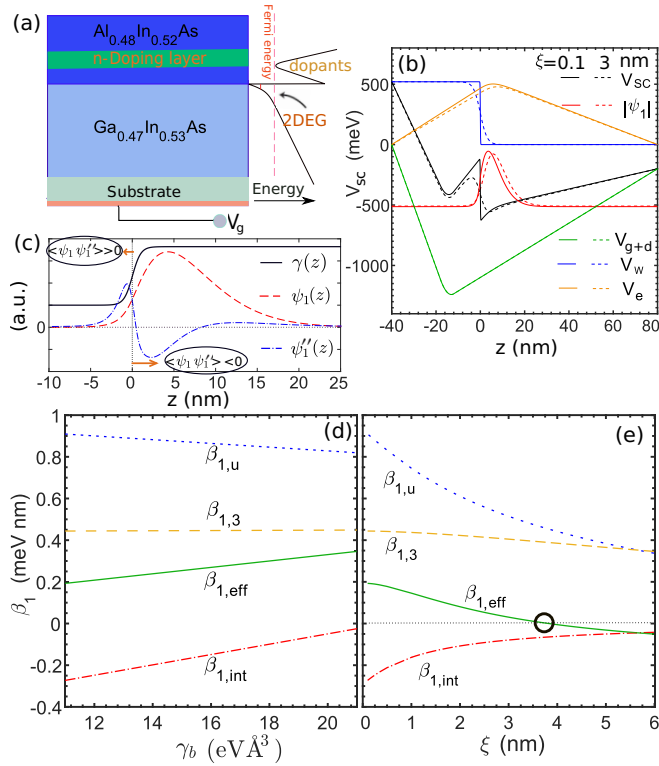


FIG. 1. (a) Growth profile (left) of an n -doped $\text{Al}_{0.48}\text{In}_{0.52}\text{As}/\text{Ga}_{0.47}\text{In}_{0.53}\text{As}$ heterostructure and the band structure (right) with only one occupied subband, where V_g denotes the external gate potential; vertical lines indicate the subband energy (solid) and Fermi level (dashed). (b) Self-consistent potential V_{sc} ($=V_w + V_{g+d} + V_e$) and wave function profile ψ_1 of the first subband for the heterostructure at $V_g = -0.2$ eV with interface smoothness of $\xi = 0.1$ nm (dotted curves) and 3 nm (solid curves). (c) Functional profile of $\gamma(z)$, $\psi_1(z)$, and $\psi_1'(z)$ near the two-dimensional electron gas (2DEG) region at $\xi = 1$ nm. (d) Dresselhaus SO coefficients including $\beta_{1,u}$, $\beta_{1,int}$, $\beta_{1,3}$, and $\beta_{1,eff}$ ($=\beta_{1,u} + \beta_{1,int} - \beta_{1,3}$) as functions of γ_b . (e) Dependence of relevant SO strengths on ξ . In (d), $\xi = 0.1$ nm; in (e), $\gamma_b = 11$ eV \AA^3 . The black circle in (e) indicates vanishing $\beta_{1,eff}$ at $\xi \sim 3.8$ nm. The Fermi energy is held fixed at $E_F = -0.45$ eV so that only the first subband is occupied.

on the interfacial effect and the parity of wave functions, are also discussed.

A. System and parameters

We consider $\text{Al}_{0.48}\text{In}_{0.52}\text{As}/\text{Ga}_{0.47}\text{In}_{0.53}\text{As}$ single and double heterostructures grown along the (001) direction [left panel of Fig. 1(a)], similar to experimental samples of Ref. [45].

For the SH configuration, the ionized dopants of width 6 nm in the $\text{Al}_{0.48}\text{In}_{0.52}$ layer [Fig. 1(a)] sit 18 nm away from where the heterojunction (interface) lies, with the doping density $\rho_d = 8.0 \times 10^{18} \text{ cm}^{-3}$. To facilitate our discussions in a comparative manner with the SH case, which obviously has structural inversion asymmetry, we consider in the DH configuration an asymmetric doping condition with doping densities $\rho_{d1} = 5.2 \times 10^{18} \text{ cm}^{-3}$ and $\rho_{d2} = 4.0 \times 10^{18} \text{ cm}^{-3}$ on the two sides of the doping layers, respectively. The temperature

is 0.3 K. We should emphasize that the effect of temperature in our calculation mainly enters the Fermi-Dirac distribution [15,46], which favors the occupation of higher-energy subbands at a high temperature. Strictly speaking, although the band parameters and the Kane parameters involved in the Kane model also depend on temperature [39,47], we have recently verified that these effects only provide negligible corrections to the SO couplings [48]. Therefore, our results are essentially also valid for temperatures above 0.3 K within a regime that the higher third subband remains unoccupied. When the third subband starts to be occupied by electrons, there will be more emerging SO contributions of intra- and intersubband kinds [49].

By adjusting the Fermi level (E_F) or the external gate potential (V_g), one can control the subband occupations of heterostructures. Note that (i) for a given quantum system, E_F is pinned at a constant to determine our self-consistent outcome [15,21], e.g., the electron density and so the corresponding Hartree potential, and (ii) V_g is adopted for a simultaneous tuning of the electron occupancy and the symmetry of heterostructures [17,50]. The right-hand panel of Fig. 1(a) shows the schematic of the potential profile of the layered system.

The offset at the heterojunction is chosen as $\delta_c = 0.52$ eV [21,51]. The effective electron masses of different layers forming the heterostructure are $m^*(\text{Al}_{0.48}\text{In}_{0.52}\text{As}) = 0.073m_0$ and $m^*(\text{Ga}_{0.47}\text{In}_{0.53}\text{As}) = 0.043m_0$ [21,51], respectively, with m_0 the bare electron mass. The distinction of effective masses is involved in the Ben Daniel–Duke equation [17,41], from which we determine spin-degenerate eigen-solutions used for obtaining the effective 2D model with Dresselhaus SO terms of both intra- and intersubband types (Sec. II).

The exact value of the bulk Dresselhaus parameter γ is controversial in both theory and experiment; e.g., its value in GaAs ranges from 8.5 to 30 eV \AA^3 [39,42]. To proceed in exploring the interfacial effect, we take $\gamma_w = 23$ eV \AA^3 [21] in the $\text{Ga}_{0.47}\text{In}_{0.53}\text{As}$ layer, and vary γ_b in the $\text{Al}_{0.48}\text{In}_{0.52}\text{As}$ barrier layer [52] to determine how the interface-associated Dresselhaus SO terms depend on γ_b . Furthermore, we introduce the hyperbolic tangent function to describe the structural potential, $V_w(z) = \delta_c [1 - \tanh(z/\xi)]/2$, of a single heterostructure with the interface located at $z = 0$. Here the parameter ξ characterizes the interface smoothness, allowing us to treat it as an adjustable parameter for exploring more thoroughly the interfacial effect on the Dresselhaus SO coupling. Clearly, the interface tends to become steeper as ξ decreases and $V_w(z)$ approaches the profile of the Heaviside step function when $\xi \sim 0.1$ nm [Fig. 1(b)].

B. Self-consistent outcome

In Fig. 1(b), we show the self-consistent potential V_{sc} including several distinct constituents, i.e., V_w , V_{g+d} ($=V_g + V_d$) and V_e , as well as the wave-function profiles ψ_v ($v = 1, 2$) for the single $\text{Al}_{0.48}\text{In}_{0.52}\text{As}/\text{Ga}_{0.47}\text{In}_{0.53}\text{As}$ heterostructure with two cases of smoothness, $\xi = 0.1$ nm (solid curves) and 3 nm (dashed curves). The structural potential V_w exhibits the usual step-function profile for the interface at $\xi = 0.1$ nm, and, as ξ increases, the potential jump from one layer to the other due to

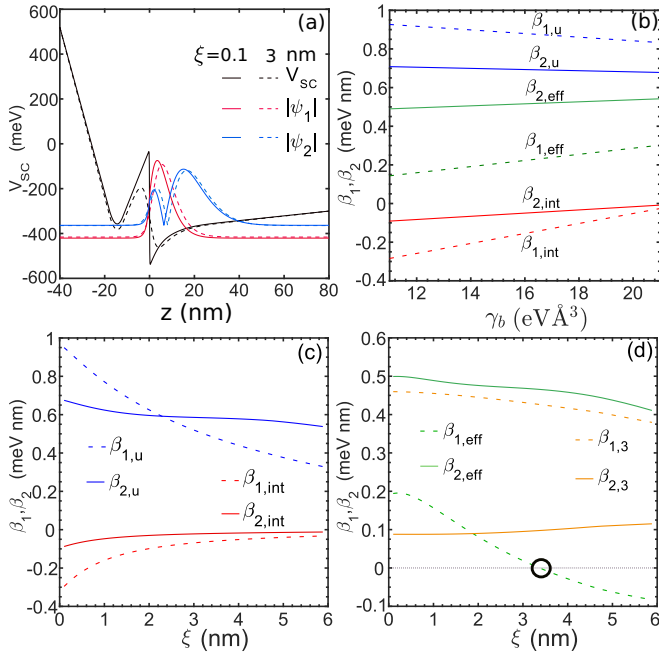


FIG. 2. (a) Self-consistent potential V_{sc} and wave function profiles ψ_ν ($\nu = 1, 2$) for a $\text{Al}_{0.48}\text{In}_{0.52}\text{As}/\text{Ga}_{0.47}\text{In}_{0.53}\text{As}$ heterostructure with $\xi = 0.1$ (solid curves) and 3 (dashed curves) at $V_g = -0.3$ eV. (b–d) Dresselhaus SO coefficients of the two subbands including $\beta_{\nu,u}$, $\beta_{\nu,int}$, $\beta_{\nu,3}$, and $\beta_{\nu,eff}$ ($=\beta_{\nu,u} + \beta_{\nu,int} - \beta_{\nu,3}$) as functions of (b) γ_b and (c, d) ξ . In (b), $\xi = 0.1$ nm; the cubic contribution $\beta_{\nu,3}$ is not shown as it is essentially independent of γ_b [see Fig. 1(c)]; in (c) and (d), $\gamma_b = 11$ eV \AA^3 ; the black circle indicates that $\beta_{2,eff}$ is vanishing at $\xi \sim 3.4$ nm. The Fermi level is set at $E_F = -0.35$ eV, ensuring that there are two occupied electron subbands.

the band offset becomes more smooth. Thus, it is reasonable to set ξ as a parameter characterizing the interface smoothness (cf. V_w at $\xi = 0.1$ and 3 nm). The gate plus doping potential V_{g+d} entirely depends on the doping condition and the external gate, and hence maintains invariance with respect to ξ . In contrast, the interface smoothness may affect the electron Hartree potential V_e as it modifies our self-consistent outcome and so the electron charge density (cf. V_{g+d} and V_e).

Figure 1(c) shows the distributional profiles of $\gamma(z)$, $\psi_1(z)$ and its second derivative with respect to z [i.e., $\psi_1''(z)$], which are the essential quantities determining the Dresselhaus SO terms [Eqs. (9)–(15)]. Here we present a case of the heterostructure having a relatively smooth interface with $\xi = 1$ nm for better illustrating the distributional profile of relevant quantities, without lack of generality. It is found that the averaged value of $\psi_1(z)\psi_1''(z)$, i.e., $\langle\psi_1(z)\psi_1''(z)\rangle$, which associates with the expectation value of k_z^2 , is greater and less than zero when $z < 0$ and $z > 0$, respectively. These self-consistent outcomes, including more of others that we analyze below [see Figs. 2(a), 3(a), and 3(b)], are helpful in elucidating our calculated SO couplings.

C. Interface-mediated Dresselhaus SO couplings

1. Single occupancy

In Fig. 1(d), we show the interface-associated Dresselhaus couplings as functions of γ_b for the heterostructure having only one occupied subband. We first look into the usual linear

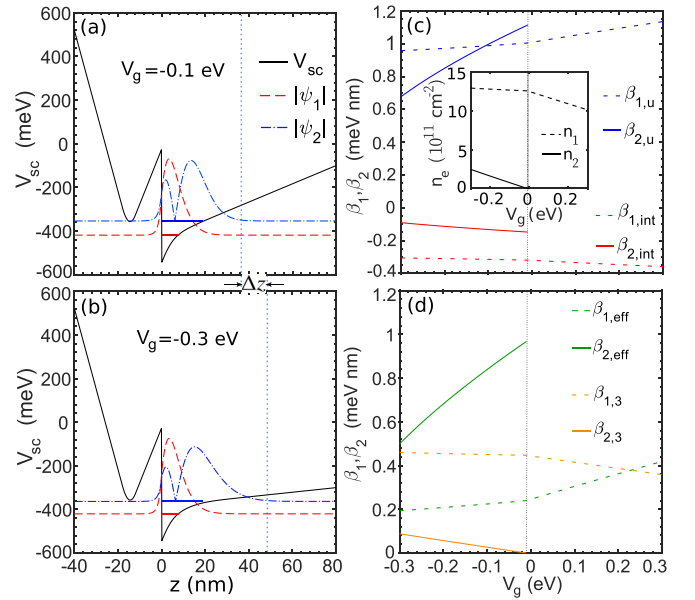


FIG. 3. Self-consistent potential V_{sc} and wave-function profiles ψ_ν for the $\text{Al}_{0.48}\text{In}_{0.52}\text{As}/\text{Ga}_{0.47}\text{In}_{0.53}\text{As}$ heterostructure with $\xi = 0.1$ nm at (a) $V_g = -0.1$ eV and (b) $V_g = -0.3$ eV. The horizontal lines inside the heterostructural confinement indicate the subband energy levels \mathcal{E}_1 and \mathcal{E}_2 . (a) $\mathcal{E}_1 = -420.6$ meV, $\mathcal{E}_2 = -363.5$ meV; in (b), $\mathcal{E}_1 = -419.1$ meV, $\mathcal{E}_2 = -354.1$ meV. (c, d) Dresselhaus SO coefficients as functions of V_g , with the inset in (c) showing the gate dependence of subband occupations n_ν with $n_e = n_1 + n_2$. In (a) and (b), the vertical dotted line indicates where the second-subband wave function vanishes, with Δz a shift between two biases of $V_g = -0.3$ and -0.1 eV; in (c) and (d), the vertical dotted line at $V_g \sim -0.01$ eV marks a transition from single to double electron occupancy. The Fermi energy is held fixed at $E_F = -0.35$ eV so that there are two occupied electron subbands.

and cubic terms. We observe that the usual linear Dresselhaus SO coefficient $\beta_{1,u} = \langle\psi_1|\gamma(z)k_z^2|\psi_1\rangle$ decreases (though slightly) with the increasing of γ_b , in contrast to the usual scenario in which the increasing of bulk Dresselhaus constant is expected to enhance the SO strength. This unusual feature follows directly from our self-consistent outcome of the sign reversal of the quantity $\langle\psi_1(z)\psi_1''(z)\rangle$ across the interface [Fig. 1(c)], making γ_w and γ_b have compensated contributions to $\beta_{1,u}$. Regarding the cubic term, since the electrons are mostly confined in the $\text{Ga}_{0.47}\text{In}_{0.53}\text{As}$ layer [Fig. 1(b)], which has a lower potential energy for electrons, which leads to $\langle\gamma(z)\rangle \sim \gamma_w$, it straightforwardly follows that $\beta_{1,3}$ remains essentially constant when γ_b varies. We should note that the slight reduction of $\beta_{1,u}$ with γ_b is usually ignored in the literature, where $\gamma(z)$ is assumed layer independent by setting it equal to γ_w throughout the entire system.

Now we turn to the interface term $\beta_{1,int}$. For a step-function profiled interface, it is straightforward to obtain from Eq. (13) a more expanded form, with $\beta_{1,int} = \psi_1(z=0)[\gamma_b\psi_1'(z=0^-) - \gamma_w\psi_1'(z=0^+)]$, in which $z = 0$ is where the interface lies. Depending on the interplay of the quantities γ_w , γ_b , and $\psi_1'(z)$, with $\psi_1'(z)$ obeying the matching condition of $(1/m_b)\psi_1'(0^-) = (1/m_w)\psi_1'(0^+)$ at the interface [53], $\beta_{1,int}$ may have opposite signs to the usual linear and cubic terms [Fig. 1(d)] [54]. For the renormalized term $\beta_{1,eff}$, it essentially

increases linearly with γ_b , following from the combined dependence of $\beta_{1,u}$, $\beta_{1,int}$ and $\beta_{1,3}$ on γ_b (Sec. II C).

Figure 1(e) shows the dependence of Dresselhaus SO coefficients on the interface smoothness. To perform our numerical simulation on heterostructures with interfaces of different smoothness, we consider the structural potential having the functional form of $V_w(z) = \delta_c [1 - \tanh(z/\xi)]/2$ [55] (Sec. III A), and similarly for other essential layer-dependent physical quantities including the bulk Dresselhaus parameter $\gamma(z) = (\gamma_b + \gamma_w)/2 + [(\gamma_w - \gamma_b)/2] \tanh(z/\xi)$ and the effective electron mass $m(z) = (m_b + m_w)/2 + [(m_w - m_b)/2] \tanh(z/\xi)$ [55], where the parameter ξ characterizes the interface smoothness and the indices “b” and “w” separately denote the barrier and well layers. Furthermore, when we determine $\beta_{v,int}$ [Eq. (10)], in order to avoid an unexpected numerical deficit in dealing with the term $\gamma_{int}(z)$, which involves the derivative of $\gamma(z)$ with respect to z and tends to be a δ function for small values of ξ , we resort to the original Ben Daniel–Duke equation [17,41] and compute $\beta_{v,int}$ through a trick, as shown in the Appendix. We find that $\beta_{1,int}$ decreases greatly with the increasing of ξ , indicating that the interfacial effect gets to be quenched for heterostructures having a smoother interface, as expected. Similarly, the usual linear term $\beta_{1,u}$ also becomes weakened with growing ξ as a larger smoothness of heterostructures implies a weaker quantum confinement for electrons. As for the cubic term $\beta_{1,3}$, it is weakly dependent of the interface smoothness. Remarkably, we observe that the renormalized linear Dresselhaus SO coefficient $\beta_{1,eff}$ may vanish at around $\xi = 3.4$ nm and further change the sign (see the black circle). This opens up more possibilities of manipulating the intriguing state of the persistent spin helix [56–59].

As a remark, to describe the interface smoothness, in addition to the form of hyperbolic tangent function that was widely adopted in the literature [55,60–63], one can also resort to the Gaussian profile [64]. Our main conclusion about the interface effect does not depend on the choice of $V_w(z)$ [and $\gamma(z)$] in describing the smoothness. For either choice, the interface becomes the step-function-like profile in the abrupt case and the offset near the heterojunction tends to vanish when the interface is smooth enough. Most importantly, the interface effect gets quenched with increasing smoothness, as discussed above, which is physically reasonable. Furthermore, experimentally, the interface smoothness can be realized by alloy composition and architecture [60–63] for exploring the interface-mediated SO couplings in future.

2. Double occupancy

Now we focus on the heterostructure having two occupied electron subbands, which can be directly achieved by increasing the Fermi level or lifting the external gate potential energy. In Fig. 2(a), we show the corresponding self-consistent potential V_{sc} and the wave-function profiles of ψ_v of the two subbands for heterostructures with interface smoothness $\xi = 0.1$ and 3 nm. As mentioned in Sec. III C 1, a larger interface smoothness represents a weaker quantum confinement for electrons. This can also be seen from the distributional profile of ψ_v in Fig. 2(a), where the wave function spreads more for a larger value of ξ away from the interface [cf. ψ_v at $\xi = 0.1$ nm (solid curves) and 3 nm (dotted curves)].

Moreover, ψ_1 has a more sensitive dependence on ξ than ψ_2 , as electrons occupying the first (lowest) subband *feel* more straightforward for the interface-engineering-induced modifications of the confinement potential.

Similar to the case of single electron occupancy, we first look into how the bulk Dresselhaus parameter γ_b of the barrier layer affects relevant SO terms including $\beta_{v,u}$, $\beta_{v,int}$, and $\beta_{v,eff}$, as shown in Fig. 2(b). Note that the cubic contribution $\beta_{v,3}$ is not shown as it is essentially independent of γ_b [Fig. 1(c)]. On the one hand, the basic behavior of relevant SO terms as functions of γ_b is found similar to that when there is only one occupied subband; on the other hand, all the relevant SO terms of the second subband have much weaker dependence on γ_b than those of the first subband. This straightforwardly follows from the fact that ψ_1 has more penetration than ψ_2 into the barrier layer, enhancing (quenching) the dependence of SO terms on γ_b of the first (second) subband.

In Figs. 2(c) and 2(d), we show the Dresselhaus SO coefficients as functions of ξ for heterostructures having two occupied subbands. We find that $\beta_{1,u}$ decreases more abruptly than $\beta_{2,u}$. This is a direct consequence of the self-consistent outcome that ψ_1 more sensitively depends on ξ than ψ_2 [Fig. 3(a)]; i.e., ψ_1 spreads more than ψ_2 as ξ increases. As for the other SO terms including the interface contribution ($\beta_{v,int}$), the SO coefficients of the second subband also have a more sensitive dependence on ξ than the ones of the first subband. Interestingly, for the renormalized Dresselhaus SO terms, we find that $\beta_{1,eff}$ may have opposite signs to $\beta_{2,eff}$ when ξ is greater than 3.4 nm [see the black circle in Fig. 2(d)]. This gives rise to the feasibility of creating in conventional semiconductors the *interface-engineered* topological matter of persistent skyrmion lattices [14], which requires compensated SO strengths of the Rashba and renormalized Dresselhaus terms, with the two terms having opposite signs for one of the two subbands and the same sign for the other subband, i.e., $\alpha_1 = \pm\beta_{1,eff}$ and $\alpha_2 = \mp\beta_{2,eff}$. Note that here it is possible to attain the persistent skyrmion lattice (PSL) regime by engineering the interface effect at a fixed gate potential. This together with the electrical manner that we adopted before [14] makes the manipulation of the PSL state more flexible. For more details about the matching of Rashba and Dresselhaus SO strengths, see Sec. III E, in which the effect of random Rashba coupling is also discussed.

It is worth noting that the bulk Dresselhaus parameter γ is usually extracted from experiment. For instance, Walser *et al.* obtained $\gamma \sim 11$ eV \AA^3 for GaAs-based quantum wells of different widths [65]. This is also consistent with our recent work, in which we extracted essentially the same value of $\gamma \sim 11$ eV \AA^3 for GaAs wells of distinct configurations by combining theoretical simulation and experimental measurements [15]. Since the usual Dresselhaus term and the interface term have the same SO form, the interface term may get absorbed in a changed value of γ extracted from the experiment, providing an extra leverage for extracting reliable bulk Dresselhaus SO parameters.

3. Electrical Dresselhaus SO control

Below we turn to the electrical control of the interface-mediated Dresselhaus SO terms. To facilitate

our discussions, we first look into how our self-consistent outcome varies when the external gate potential changes. In Figs. 3(a) and 3(b), we show the self-consistent potential V_{sc} and the wave-function profiles ψ_ν at $V_g = -0.1$ and -0.3 eV, respectively. In contrast to the interface smoothness dependence of electron distributions [Fig. 2(a)], for the gate dependence it is found that ψ_1 is more weakly dependent on V_g than ψ_2 , following from the energy level of the first subband being deeper than that of the second subband. Specifically, when V_g varies from -0.1 to -0.3 eV, we find that ψ_1 remains essentially invariant with V_g while ψ_2 becomes more localized, with the effective-confinement width quenched roughly by $\Delta z \sim 11$ nm [cf. Figs. 3(a) and 3(b)]. This feature is helpful for elucidating the gate dependence of our computed SO terms, as we analyze next.

Figures 3(c) and 3(d) show the electric control of relevant Dresselhaus SO terms, with the inset in Fig. 3(c) illustrating how the subband occupation varies as a function of V_g , from which a simultaneous tuning of the SO strength and electron occupancy can be achieved. The vertical (dotted) line at $V_g \sim -0.025$ eV marks a transition of the electron occupancy from two subbands to one subband as V_g increases. Remarkably, when $V_g < -0.025$ eV (double occupancy), we observe that $\beta_{2,u}$ increases more abruptly than $\beta_{1,u}$, giving rise to three distinct scenarios of $\beta_{1,u} < \beta_{2,u}$, $\beta_{1,u} = \beta_{2,u}$, and $\beta_{1,u} > \beta_{2,u}$, which are fully controlled in the electrical manner, greatly facilitating selective SO control of distinct subbands. This directly follows from the feature of our self-consistent outcome that ψ_1 has much weaker dependence on V_g than ψ_2 . As a consequence, $\beta_{2,eff}$ containing $\beta_{2,u}$ as a constituent also has a strong dependence on V_g , in contrast to $\beta_{1,eff}$, which is weakly dependent of V_g . Note that one can in general realize the electrical control of $\beta_{v,eff}$ by adjusting $\beta_{v,3}$ ($\propto n_v$), which depends on the subband occupation, through an external gate [15]. Here we achieve a flexible control of $\beta_{2,eff}$ mainly by electrically varying $\beta_{2,u}$, which in general is immune to V_g [14,15]. On the other hand, we observe that the interface SO term $\beta_{v,int}$ of either subband, which mainly depends on the interfacial details (e.g., interface smoothness), exhibits weak gate dependence.

For completeness, we also examine the gate dependence of interface-mediated Dresselhaus SO couplings for heterostructures in the DH configuration, i.e., an ordinary quantum well, as shown in Figs. 4(a) and 4(b). For the usual linear term $\beta_{v,u}$, we observe contrasting features of the SO control to the case of the SH configuration. First, as usual, $\beta_{v,u}$, which mainly depends on quantum confinement, remains essentially constant with V_g . Also, the inequality $\beta_{2,u} > \beta_{1,u}$ maintains in the entire gate-voltage ranges considered. These are in distinct contrast to the SO features in the SH configuration [cf. Figs. 3(c) and 4(a)]. On the other hand, for the other interface-involved Dresselhaus SO contributions including the interface term $\beta_{v,int}$ and the cubic term $\beta_{v,3}$, the corresponding gate dependence is similar to that for heterostructures in the SH configuration.

Now, we turn to the intersubband Dresselhaus SO control. In Figs. 5(a) and 5(b), we show relevant intersubband SO terms as functions of V_g for heterostructures in the SH and DH configurations, respectively. Due to the triangular-type confinement in the SH configuration [e.g., Figs. 1(b) and 2(a)],

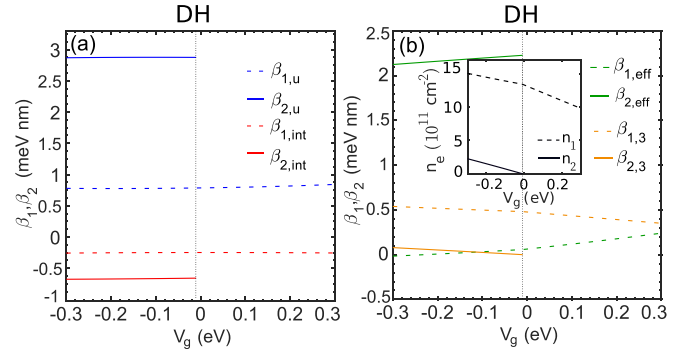


FIG. 4. Dresselhaus SO coefficients of the two subbands including (a) $\beta_{v,u}$ and $\beta_{v,int}$ and (b) $\beta_{v,3}$ and $\beta_{v,eff}$ ($=\beta_{v,u} + \beta_{v,int} - \beta_{v,3}$) for $\text{Al}_{0.48}\text{In}_{0.52}\text{As}/\text{Ga}_{0.47}\text{In}_{0.53}\text{As}$ double heterostructures (i.e., quantum well) with $\xi = 0.1$ nm as functions of V_g . The inset in (b) shows how the subband occupation n_v with $n_e = n_1 + n_2$ varies as a function of V_g . In (a) and (b), the vertical dotted line at about $V_g = -0.01$ eV marks a transition of the electron occupancy from one to two subbands. The width of the well is 14 nm and the Fermi energy is held fixed at $E_F = -0.31$ eV so that there are two occupied electron subbands.

which greatly breaks the intrinsic even or odd parities of the wave functions of the two subbands, the intersubband SO terms are much stronger than the corresponding analogs in the DH configuration with the structural potential V_w having the symmetric profile of a square well. Note that since the SH configuration is entirely spatially asymmetric, we consider the quantum well of the DH configuration being asymmetrically doped (Sec. III A), to facilitate comparisons of SO terms in the two configurations. Interestingly, in spite of the asymmetric doping condition for the DH case, we observe when

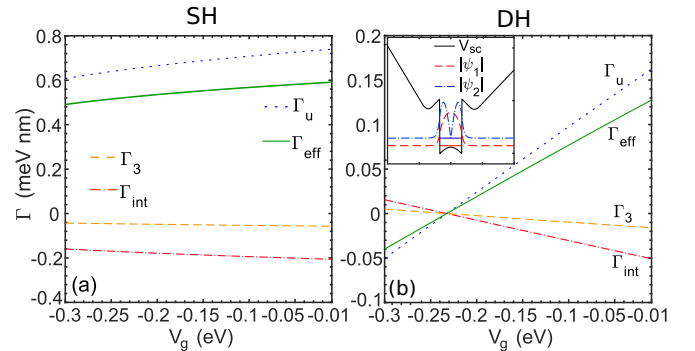


FIG. 5. Intersubband Dresselhaus SO coefficients including Γ_u , Γ_{int} , Γ_3 , and Γ_{eff} ($=\Gamma_u + \Gamma_{int} - \Gamma_3$) as functions of V_g for the $\text{Al}_{0.48}\text{In}_{0.52}\text{As}/\text{Ga}_{0.47}\text{In}_{0.53}\text{As}$ (a) single and (b) double heterostructures with $\xi = 0.1$ nm. In (b), the inset shows the self-consistent potential energy V_{sc} and wave-function profiles ψ_ν ($\nu = 1, 2$) for the double heterostructures with $V_g = -0.023$ eV, at which an effective local symmetric configuration near the well (2DEG) region occurs even though the overall system is clearly asymmetric. This local symmetric configuration comes from the compensated contributions to symmetry breaking from the external gate and asymmetric doping condition. The Fermi energy is held fixed at $E_F = -0.31$ eV so that there are two occupied electron subbands. The well width in the DH configuration is 14 nm.

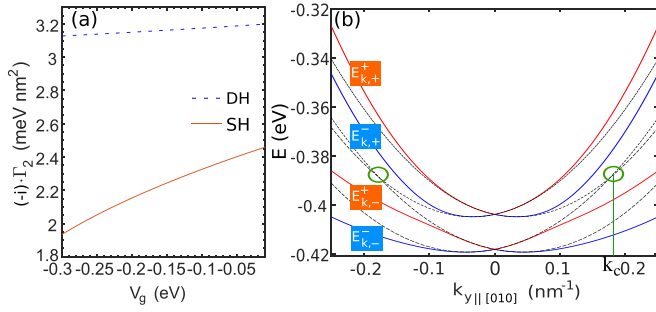


FIG. 6. (a) The quadratic intersubband Dresselhaus SO term as a function of V_g for $\text{Al}_{0.48}\text{In}_{0.52}\text{As}/\text{Ga}_{0.47}\text{In}_{0.53}\text{As}$ both single (solid curves) and double (dotted curves) heterostructures with $\xi = 0.1$ nm. (b) Avoided crossings of energy dispersion (scaled by a factor of two orders for visibility) of the four spin branches (two for each subband) $E_{k,\lambda_1}^{\lambda_2}$ along the $k_{y||[010]}$ direction when $\Gamma_2 \neq 0$ and $\Gamma \neq 0$. The black dashed lines are for the case in the absence of quadratic terms, indicating the crossing remains when $\Gamma_2 = 0$ even when $\Gamma \neq 0$. The SO constants are chosen at $V_g = -0.3$ eV for the single heterostructure (see Figs. 3 and 5).

$V_g \sim -0.025$ eV a *local* symmetric geometry near the well region, arising from compensated contributions of the asymmetric doping condition and external gate to the symmetry breaking. Furthermore, in this configuration embracing *local* space inversion symmetry, the intersubband SO terms including Γ_u , Γ_3 , Γ_{int} , and Γ_{eff} ($=\Gamma_u + \Gamma_{\text{int}} - \Gamma_3$) identically vanish because of distinct parities of wave functions of different subbands. Strictly speaking, note that the quantum well in this local symmetric configuration is actually asymmetric from the perspective of the overall system, due to the unbalanced doping conditions considered (Sec. III A).

D. Unusual avoided crossings induced by the quadratic interface Dresselhaus SO term

Finally, we move to the unusual intersubband quadratic term Γ_2 as well as the associated novel features that it induced in the energy dispersion. We first have a look at its gate dependence, as shown in Fig. 6(a) for both the single (solid curves) and double (dotted curves) heterostructures. We find that the quadratic term is weaker in the SH configuration than that in the DH one, following from the fact that it is nonzero even in the symmetric geometry due to distinct parities of the two-subband wave functions [Eq. (15)]. In other words, the two interfaces of the system in the DH configuration exhibit a *constructive* interplay in enhancing the quadratic SO contribution. This is in stark contrast to the other intersubband terms (i.e., Γ_u and Γ_3) aforementioned, which identically vanish even in a configuration which is locally symmetric. On the other hand, we observe that the quadratic term has a relatively stronger gate dependence in the former (SH) configuration.

In Fig. 6(b), we show the energy dispersion $E_{k,\lambda_1}^{\lambda_2}$, which can be obtained by solving Eq. (8), of the four spin branches (two for each subband) associated with two occupied subbands. Here $\lambda_1 = \pm 1$ and $\lambda_2 = \pm 1$ represent the pseudospin (subband) and real spin, respectively. Regarding the usual Dresselhaus model in the absence of the interfacial effect, even under the impact of intersubband term (Γ_u), the spin

branches of the two subbands remain crossed [see the dotted (black) lines]. The underlying physics is that the usual linear intersubband term only couples the same spin branches of the two subbands, which is also true for the pure Rashba model [17]. Interestingly, in the presence of Γ_2 , which depends on the interfacial effect and the parity of wave functions, we reveal that it may induce unusual anticrossings of the band dispersion [see the solid (blue and red) lines for $E_{k,-}^-$, $E_{k,-}^+$, $E_{k,+}^-$, and $E_{k,+}^+$ for the four spin (and subband) branches]. We should emphasize that the avoided crossings induced by the quadratic SO contribution may hybridize the energy branches of distinct spins and further induce novel spin textures, in contrast to the effect of the usual linear intersubband term. These features are worth exploring in a future work.

E. Rashba SO coupling

1. Matching Rashba and Dresselhaus SO strengths

The interplay of Rashba and Dresselhaus SO couplings may lead to intriguing features [14,56,57]. In particular, when the strengths of the Rashba (α_v) and Dresselhaus ($\beta_{v,\text{eff}}$) constants match, the competing effects of two distinct SO interactions (Rashba and Dresselhaus) can (partially) cancel each other out, thus reducing spin decay. In this case, a robust spin-density wave excitation of persistent spin helix may emerge in 2D electron gases [56–59]. Also, we recently revealed that quantum wells with two subbands can sustain an intriguing spin texture of a persistent skyrmion lattice with topological properties when $\alpha_1 = \pm\beta_{1,\text{eff}}$ and $\alpha_2 = \mp\beta_{2,\text{eff}}$ [14].

For quantum wells with only one occupied subband, the persistent spin helix has been observed experimentally by means of spin-grating spectroscopy [58], and via time- and spatially resolved magneto-optical Kerr rotation [59,66]. And recently, we even realized the continuous locking of the SO fields at $\alpha_1 = \beta_{1,\text{eff}}$, which makes possible the concept of *stretchable* spin helices. Thus, here we mainly focus on the challenging case of double electron occupancy. In Fig. 7(a) [Fig. 7(b)], we show the Rashba and the renormalized Dresselhaus SO strengths for our 14-nm quantum well with two occupied subbands as functions of V_g (ξ) [67]. Since the well is relatively narrow, in the parameter range considered we only achieve the matching Rashba and Dresselhaus strengths for the first subband, i.e., $\alpha_1 = \beta_{1,\text{eff}}$ (see black circle), while for the second subband $\beta_{2,\text{eff}}$ is much greater than α_2 . It is interesting to note that at $V_g \sim -0.22$ eV the relation $\alpha_1 = \beta_{1,\text{eff}}$ (though the strength is quite weak) essentially remains for all values of smoothness considered [see Fig. 7(b)]. To *simultaneously* have $\alpha_1 = \pm\beta_{1,\text{eff}}$ and $\alpha_2 = \mp\beta_{2,\text{eff}}$ in the regime of persistent skyrmion lattice, one can in principle resort to a wider quantum well which has smaller $\beta_{2,\text{eff}}$ or a double-well configuration. In the latter double-well case, we show the dependence of α_v and $\beta_{v,\text{eff}}$ on V_g (ξ) in Fig. 7(c) [Fig. 7(d)], and the matching of Rashba and Dresselhaus strengths is indicated by black circles. For more details about our self-consistent procedure in evaluating the the Rashba coupling comprising contributions from the gate potential (V_g), doping potential (V_d), electron Hartree potential (V_e), and structural potential (V_w), see Refs. [14,15,46].

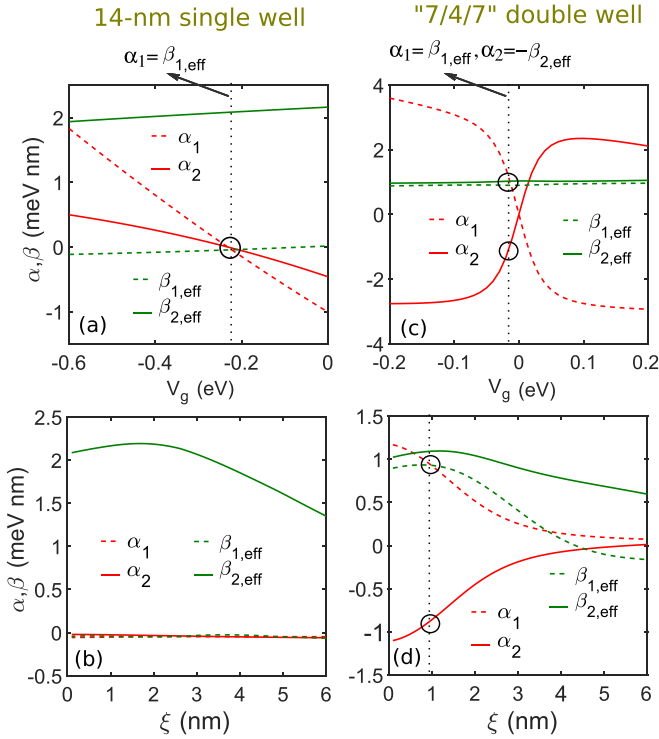


FIG. 7. Rashba α_v and Dresselhaus $\beta_{v,\text{eff}}$ ($=\beta_{v,u} + \beta_{v,\text{int}} - \beta_{v,3}$) ($v = 1, 2$) SO coupling constants for the $\text{Al}_{0.48}\text{In}_{0.52}\text{As}/\text{Ga}_{0.47}\text{In}_{0.53}\text{As}$ single well of width equal to 14 nm as functions of (a) V_g at $\xi = 0.1$ nm and of (b) ξ at $V_g = -0.22$ eV. (c, d) Dependence of Rashba and Dresselhaus coefficients on (c) V_g at $\xi = 0.1$ nm and (d) ξ at $V_g = -0.016$ eV for a “7/4/7” double well, with the numbers 7 and 4 denoting the width of the two local (left and right) wells (7 nm) and of the central barrier (4 nm), respectively. The black circles indicate where the matching of α_v and $\beta_{v,\text{eff}}$ occurs. Note that in (b) α_v (though it is small) essentially matches $\beta_{v,\text{eff}}$ for all values of smoothness (ξ) considered. In (a) and (b), the Fermi level is held fixed at $E_F = -0.35$ eV; in (c) and (d), we set $E_F = 0$.

2. Random Rashba coupling

Fluctuations of the concentration of dopant ions could lead to a random electric field along the growth direction of heterostructures [68,69], and hence a random Rashba coupling [68–72]. We follow Ref. [68] and evaluate the averaged random Rashba SO strength $\sqrt{\langle \alpha_{v,R}^2 \rangle} = e^2 \xi \sqrt{\pi n_d} / 4\pi \epsilon R_d$, with the subscript R indicating the random contribution. Here e is the electron charge, ϵ denotes the dielectric constant, R_d refers to the distance from the doping region to the well center, and ξ is a Rashba parameter depending on bulk quantities of materials [15,46]. As electrons of the two subbands see the same doping conditions, fluctuations of the Rashba couplings are assumed the same in both subbands. For our quantum heterostructures, we obtain $\sqrt{\langle \alpha_{v,R}^2 \rangle} \sim 0.1\alpha_v$. The random Rashba coupling may modify the matching condition of the persistent spin helix and skyrmion lattice. Depending on specific applications, one can enhance (quench) the random Rashba effect by increasing (decreasing) the doping concentration and/or by setting the

doping region near (distant from) the region of 2D electron gases.

IV. CONCLUDING REMARKS

Starting from the bulk crystal to heterostructures, we have explored systematically the interface-mediated Dresselhaus spin-orbit (SO) couplings including the usual linear and cubic contributions as well as the interface terms of both intra- and intersubband kinds. We consider $\text{Al}_{0.48}\text{In}_{0.52}\text{As}/\text{Ga}_{0.47}\text{In}_{0.53}\text{As}$ heterostructures both single and double heterostructures with either one or two occupied subbands ($v = 1, 2$). By varying the bulk Dresselhaus parameter γ_b in the barrier layer and introducing the interface smoothness coefficient ξ , we have determined how the relevant SO terms depend on γ_b and ξ . We observe that the interface SO term may be comparable with the usual ones and becomes more important at either a lower interface smoothness near the heterojunction or a weaker bulk Dresselhaus strength of the barrier layer. Remarkably, it is found that the renormalized Dresselhaus coefficient may change sign as the interface smoothness varies, opening a feasibility of generating *interface-engineered* topological matter of persistent skyrmion lattice [14]. Moreover, by adjusting the gate potential, we reveal that for a *single* heterostructure the Dresselhaus coefficient of the second subband changes more abruptly than that of the first subband, giving rise to three distinct scenarios of $\beta_{1,u} < \beta_{2,u}$, $\beta_{1,u} = \beta_{2,u}$, and $\beta_{1,u} > \beta_{2,u}$, greatly fascinating for selective SO control of distinct subbands. The relevant SO features have also been compared with the case of double heterostructures, which involve the interplay of the two interfaces in the SO contributions. Moreover, we also obtain an emergent *quadratic* Dresselhaus SO term depending on the interfacial effect and the parity of wave functions. As opposed to intersubband terms of the usual linear and cubic kinds, the quadratic contribution gives rise to avoided crossings of band dispersion, which is expected to elucidate novel SO-related phenomena beyond the usual Rashba and Dresselhaus model in the absence of interfacial effect. Furthermore, the quadratic SO term may hybridize energy branches of distinct spins and further induce unusual hybridized spin textures. We point out that the interface terms are expected to be important in heterostructures with large band offset and distinct effective electron mass and bulk Dresselhaus constants between different layers. Our results should stimulate experiments probing interface-mediated SO effects and provide an extra leverage for extracting a reliable bulk Dresselhaus SO parameter, the value of which is usually controversial in both theory and experiment. Finally, hole SO coupling has also become one of the main topics of interest in quantum heterostructures owing to its rich physical phenomena [73–76] including Fermi contour anisotropy [77], exciton gases [78], and topological structures [79]. Additional work is needed to explore features of the SO coupling for holes.

ACKNOWLEDGMENTS

This work was supported by the National Natural Science Foundation of China (Grant No. 11874236) and the QFNU research fund. J.Y.F. thanks his former undergraduate student

W. C. Liu for her contribution in the early stage of this project and J. C. Egues and D. M. Zumbühl for valuable discussions about interface effects when he visited University of Sao Paulo. H.Y. thanks Wen Liu for illuminating discussions about random Rashba coupling.

APPENDIX: EVALUATION OF THE INTERFACE DRESSELHAUS SO TERM

The interface Dresselhaus SO coefficient of the intrasubband term reads

$$\beta_{v,\text{int}} = -\langle v | \gamma_{\text{int}}(z) \partial_z | v \rangle = - \int \psi_v^*(z) \gamma'(z) \psi'_v(z) dz, \quad (\text{A1})$$

where the layer-dependent parameter $\gamma(z)$ is treated in a widely adopted way of introducing the hyperbolic tangent function [55],

$$\gamma(z) = \frac{\gamma_w + \gamma_b}{2} + \frac{\gamma_w - \gamma_b}{2} \tanh\left(\frac{z}{\xi}\right). \quad (\text{A2})$$

Note that $\gamma(z)$ tends to become a Heaviside step function as ξ decreases (see Sec. III A of the main text).

By inserting Eq. (A2) into Eq. (A1), it is straightforward to obtain

$$\beta_{v,\text{int}} = -\frac{\gamma_w - \gamma_b}{2} \int \psi_v^*(z) \tanh'\left(\frac{z}{\xi}\right) \psi'_v(z) dz. \quad (\text{A3})$$

To avoid the numerical deficit when dealing with the function $\tanh'(z/\xi)$ in particular for *steep* interfaces at small values of ξ , we resort to the Ben Daniel–Duke equation [17,41], resolving the issue in a tricky manner. Specifically, the Ben Daniel–Duke model involving distinct effective electron masses of different layers is written as [17,41]

$$-\frac{\hbar^2}{2} \frac{\partial}{\partial z} \frac{1}{m(z)} \frac{\partial}{\partial z} \psi_v(z) + V_{\text{sc}}(z) \psi_v(z) = \varepsilon_v \psi_v(z), \quad (\text{A4})$$

with

$$m(z) = \frac{m_w + m_b}{2} + \frac{m_w - m_b}{2} \tanh\left(\frac{z}{\xi}\right). \quad (\text{A5})$$

By multiplying $\psi_v^*(z)$ on the left-hand side of Eq. (A4) and making integration over the space of the z direction, one obtains

$$\text{I} \equiv \int \psi_v^*(z) (\varepsilon_v - V(z)) \psi_v(z) dz = \text{II} + \text{III} + \text{IV}, \quad (\text{A6})$$

where we have defined

$$\text{II} = -\frac{\hbar^2}{4} \left(\frac{1}{m_w} + \frac{1}{m_b} \right) \int \psi_v^*(z) \psi_v''(z) dz, \quad (\text{A7})$$

$$\text{III} = -\frac{\hbar^2}{4} \left(\frac{1}{m_w} - \frac{1}{m_b} \right) \int \psi_v^*(z) \tanh\left(\frac{z}{\xi}\right) \psi_v''(z) dz, \quad (\text{A8})$$

and

$$\text{IV} = -\frac{\hbar^2}{4} \left(\frac{1}{m_w} - \frac{1}{m_b} \right) \int \psi_v^*(z) \tanh'\left(\frac{z}{\xi}\right) \psi_v'(z) dz. \quad (\text{A9})$$

From Eqs. (A6)–(A9), we rewrite the interface term [Eq. (A1)] as

$$\begin{aligned} \beta_{v,\text{int}} &= \frac{2(\gamma_w - \gamma_b)}{\hbar^2} \frac{m_w m_b}{m_b - m_w} \int \psi_v^*(z) [\varepsilon_v - V(z)] \psi_v(z) dz \\ &\quad + \frac{\gamma_w - \gamma_b}{2} \int \psi_v^*(z) \left[\frac{m_w + m_b}{m_b - m_w} + \tanh\left(\frac{z}{\xi}\right) \right] \\ &\quad \times \psi_v''(z) dz. \end{aligned} \quad (\text{A10})$$

The same procedure can be applied to evaluate the inter-subband term Γ_{int} by replacing ψ_v^* with $\psi_{v'}^*$ ($v \neq v'$), i.e., the corresponding expectation values involve the wave functions of distinct subbands.

-
- [1] D. Awschalom, D. Loss, and N. Samarth, *Semiconductor Spintronics and Quantum Computation* (Springer, New York, 2002).
- [2] I. Žutić, J. Fabian, and S. D. Sarma, Spintronics: Fundamentals and applications, *Rev. Mod. Phys.* **76**, 323 (2004).
- [3] P. Chuang, S. Ho, L. W. Smith, F. Sfigakis, M. Pepper, C. Chen, J. Fan, J. P. Griffiths, I. Farrer, H. E. Beere, G. A. C. Jones, D. A. Ritchie, and T. Chen, All-electric all-semiconductor spin field-effect transistors, *Nat. Nanotechnol.* **10**, 35 (2015).
- [4] H. C. Koo, J. H. Kwon, J. Eom, J. Chang, S. H. Han, and M. Johnson, Control of spin precession in a spin-injected field effect transistor, *Science* **325**, 1515 (2009).
- [5] S. Datta and B. Das, Electronic analog of the electro-optic modulator, *Appl. Phys. Lett.* **56**, 665 (1990).
- [6] J. Sinova, S. O. Valenzuela, J. Wunderlich, C. H. Back, and T. Jungwirth, Spin Hall effects, *Rev. Mod. Phys.* **87**, 1213 (2015).
- [7] J. Wunderlich, B. Park, A. C. Irvine, L. P. Zárbo, E. Rozkotová, P. Nemeš, V. Novák, J. Sinova, and T. Jungwirth, Spin Hall effect transistor, *Science* **30**, 1801 (2010).
- [8] H. Bentmann, S. Abdelouahed, M. Mulazzi, J. Henk, and F. Reinert, Direct Observation of Interband Spin-Orbit Coupling in a Two-Dimensional Electron System, *Phys. Rev. Lett.* **108**, 196801 (2012).
- [9] R. Noguchi, K. Kuroda, K. Yaji, K. Kobayashi, M. Sakano, A. Harasawa, T. Kondo, F. Komori, and S. Shin, Direct mapping of spin and orbital entangled wave functions under interband spin-orbit coupling of giant Rashba spin-split surface states, *Phys. Rev. B* **95**, 041111(R) (2017).
- [10] B. A. Bernevig, T. L. Hughes, and S. C. Zhang, Quantum spin Hall effect and topological phase transition in HgTe quantum wells, *Science* **314**, 1757 (2006).
- [11] R. M. Lutchyn, J. D. Sau, and S. Das Sarma, Majorana Fermions and a Topological Phase Transition in Semiconductor-Superconductor Heterostructures, *Phys. Rev. Lett.* **105**, 077001 (2010).
- [12] Y. Oreg, G. Refael, and F. Von Oppen, Helical Liquids and Majorana Bound States in Quantum Wires, *Phys. Rev. Lett.* **105**, 177002 (2010).
- [13] H. M. Weng, C. Fang, Z. Fang, B. A. Bernevig, and X. Dai, Weyl Semimetal Phase in Noncentrosymmetric Transition-Metal Monophosphides, *Phys. Rev. X* **5**, 011029 (2015).
- [14] J. Y. Fu, P. H. Penteado, M. O. Hachiya, D. Loss, and J. C. Egues, Persistent Skyrmion Lattice of Noninteracting Electrons with Spin-Orbit Coupling, *Phys. Rev. Lett.* **117**, 226401 (2016).

- [15] F. Dettwiler, J. Y. Fu, S. Mack, P. J. Weigele, J. C. Egues, D. D. Awschalom, and D. M. Zumbühl, Stretchable Persistent Spin Helices in GaAs Quantum Wells, *Phys. Rev. X* **7**, 031010 (2017).
- [16] P. J. Weigele, D. C. Marinescu, F. Dettwiler, J. Fu, S. Mack, J. C. Egues, D. D. Awschalom, and D. M. Zumbühl, Symmetry breaking of the persistent spin helix in quantum transport, *Phys. Rev. B* **101**, 035414 (2020).
- [17] Q. Wang, H. Yang, and J. Fu, Selective asymmetric gate control of the Rashba spin-orbit coupling in GaInAs/AlInAs stepped wells, *Phys. Rev. B* **101**, 245403 (2020).
- [18] F. Nichele, M. Kjaergaard, H. J. Suominen, R. Skolasinski, M. Wimmer, B. M. Nguyen, A. A. Kiselev, W. Yi, M. Sokolich, M. J. Manfra, F. Qu, A. J. A. Beukman, L. P. Kouwenhoven, and C. M. Marcus, Giant Spin-Orbit Splitting in Inverted InAs/GaSb Double Quantum Wells, *Phys. Rev. Lett.* **118**, 016801 (2017).
- [19] J. Nitta, T. Akazaki, H. Takayanagi, and T. Enoki, Gate Control of Spin-Orbit Interaction in an Inverted $\text{In}_{0.53}\text{Ga}_{0.47}\text{As}/\text{In}_{0.52}\text{Al}_{0.48}\text{As}$, *Phys. Rev. Lett.* **78**, 1335 (1997).
- [20] D. Grundler, Large Rashba Splitting in InAs Quantum Wells Due to Electron Wave Function Penetration into the Barrier Layers, *Phys. Rev. Lett.* **84**, 6074 (2000).
- [21] R. S. Calsaverini, E. Bernardes, J. C. Egues, and D. Loss, Intersubband-induced spin-orbit interaction in quantum wells, *Phys. Rev. B* **78**, 155313 (2008).
- [22] M. Kammermeier, A. Seith, P. Wenk, and J. Schliemann, Persistent spin textures and currents in wurtzite nanowire-based quantum structures, *Phys. Rev. B* **101**, 195418 (2020).
- [23] J. Y. Fu, P. H. Penteado, D. R. Candido, G. J. Ferreira, D. P. Pires, E. Bernardes, and J. C. Egues, Spin-orbit coupling in wurtzite heterostructures, *Phys. Rev. B* **101**, 134416 (2020).
- [24] Y. A. Bychkov and E. I. Rashba, Properties of a 2D electron gas with lifted spectral degeneracy, *JETP Lett.* **39**, 78 (1984).
- [25] G. Dresselhaus, Spin-orbit coupling effects in zinc blende structures, *Phys. Rev.* **100**, 580 (1955).
- [26] W. N. Lin, L. Li, F. Dogan, C. J. Li, H. Rotella, X. J. Yu, B. M. Zhang, Y. Y. Li, W. S. Lew, S. J. Wang, W. Prellier, S. J. Pennycook, Z. C. Chen, J. S. Zhong, A. Manchon, and T. Wu, Interface-based tuning of Rashba spin-orbit interaction in asymmetric oxide heterostructures with 3d electrons, *Nat. Commun.* **10**, 3052 (2019).
- [27] J. Sklenar, W. Zhang, M. B. Jungfleisch, W. J. Jiang, H. Saglam, J. E. Pearson, J. B. Ketterson, and A. Hoffmann, Perspective: Interface generation of spin-orbit torques, *J. Appl. Phys.* **120**, 180901 (2016).
- [28] V. P. Amin, J. Zemen, and M. D. Stiles, Interface-Generated Spin Currents, *Phys. Rev. Lett.* **121**, 136805 (2018).
- [29] D. Zhang, W. K. Lou, M. S. Miao, S. C. Zhang, and K. Chang, Interface-Induced Topological Insulator Transition in GaAs/Ge/GaAs Quantum Wells, *Phys. Rev. Lett.* **111**, 156402 (2013).
- [30] T. Maruyama, Y. Shiota, T. Nozaki, K. Ohta, N. Toda, M. Mizuguchi, A. A. Tulapurkar, T. Shinjo, M. Shiraishi, S. Mizukami, Y. Ando, and Y. Suzuki, Large voltage-induced magnetic anisotropy change in a few atomic layers of iron, *Nat. Nanotechnol.* **4**, 158 (2009).
- [31] F. Hellman, A. Hoffmann, Y. Tserkovnyak, G. S. D. Beach, E. E. Fullerton, C. Leighton, A. H. MacDonald, D. C. Ralph, D. A. Arena, H. A. Durr *et al.*, Interface-induced phenomena in magnetism, *Rev. Mod. Phys.* **89**, 025006 (2017).
- [32] M. Bode, M. Heide, K. Von Bergmann, P. Ferriani, S. Heinze, G. Bihlmayer, A. Kubetzka, O. Pietzsch, S. Blügel, and R. Wiesendanger, Chiral magnetic order at surfaces driven by inversion asymmetry, *Nature (London)* **447**, 190 (2007).
- [33] Y. F. Hao, Spin-orbit interaction in multiple quantum wells, *J. Appl. Phys.* **117**, 013911 (2015).
- [34] Z. A. Devizorova, A. V. Shchepetilnikov, Y. A. Nefyodov, V. A. Volkov, and I. V. Kukushkin, Interface contributions to the spin-orbit interaction parameters of electrons at the (001) GaAs/AlGaAs interface, *JETP Lett.* **100**, 102 (2014).
- [35] W. Wang, X. M. Li, and J. Y. Fu, Electrical control of the spin-orbit coupling in GaAs from single to double and triple wells, *Superlattices Microstruct.* **88**, 43 (2015).
- [36] L. Chen, M. Gmitra, M. Vogel, R. Islinger, M. Kronseder, D. Schuh, D. Bougeard, J. Fabian, D. Weiss, and C. H. Back, Electric-field control of interfacial spin-orbit fields, *Nat. Electron.* **1**, 350 (2018).
- [37] M. I. Dyakonov and V. Y. Kachorovskii, Spin relaxation of two-dimensional electrons in non-centrosymmetric semiconductors, *Sov. Phys. Semicond.* **20**, 110 (1986).
- [38] P. S. Alekseev and M. O. Nestoklon, Effective one-band approach for the spin splittings in quantum wells, *Phys. Rev. B* **95**, 125303 (2017).
- [39] J. Fabian, A. Matos-Abiague, C. Ertler, P. Stano, and I. Žutić, Semiconductor spintronics, *Acta Phys. Slovaca* **57**, 565 (2007).
- [40] Y. F. Hao, Interface effect in coupled quantum wells, *J. Appl. Phys.* **115**, 244308 (2014).
- [41] G. Bastard, *Wave Mechanics Applied to Semiconductor Heterostructures* (Halsted, Les Ulis, New York, 1989).
- [42] J.-M. Jancu, R. Scholz, E. A. De Andrada E Silva, and G. C. La Rocca, Atomistic spin-orbit coupling and $\mathbf{k}\cdot\mathbf{p}$ parameters in III-V semiconductors, *Phys. Rev. B* **72**, 193201 (2005).
- [43] W. Knap, C. Skierbiszewski, A. Zduniak, E. Litwin-Staszewska, D. Bertho, F. Kobbi, J. L. Robert, G. E. Pikus, F. G. Pikus, S. V. Iordanskii, V. Mosser, K. Zekentes, and Y. B. Lyanda-Geller, Weak antilocalization and spin precession in quantum wells, *Phys. Rev. B* **53**, 3912 (1996).
- [44] The cubic Dresselhaus SO term related to β_3 can be decomposed into sin and cos functions of θ (first harmonic) and 3θ (third harmonic), with θ the polar coordinate of the momentum \mathbf{k} in the 2DEG plane [15,80].
- [45] T. Koga, J. Nitta, T. Akazaki, and H. Takayanagi, Rashba Spin-Orbit Coupling Probed by the Weak Antilocalization Analysis in InAlAs/InGaAs/InAlAs Quantum Wells as a Function of Quantum Well Asymmetry, *Phys. Rev. Lett.* **89**, 046801 (2002).
- [46] J. Y. Fu and J. C. Egues, Spin-orbit interaction in GaAs wells: From one to two subbands, *Phys. Rev. B* **91**, 075408 (2015).
- [47] R. Winkler, *Spin-Orbit Coupling Effects in Two-Dimensional Electron and Hole Systems* (Springer, New York, 2003).
- [48] W. Wang and J. Y. Fu, Temperature dependence of the Rashba and Dresselhaus spin-orbit interactions in GaAs wells, *Phys. B: Condens. Matter* **482**, 14 (2016).
- [49] Y. Suo, H. Yang, and J. Y. Fu, Distinct three-level spin-orbit control associated with electrically controlled band swapping, *Chin. Phys. Lett.* **37**, 117101 (2020).

- [50] W. Liu, H. Yang, and J. Y. Fu, Band-crossing and anticrossing triggered unusual spin-orbit control in InSb triple wells (unpublished).
- [51] I. Vurgaftman, J. R. Meyer, and L. R. Ram-Mohan, Band parameters for III–V compound semiconductors and their alloys, *J. Appl. Phys.* **89**, 5815 (2001).
- [52] Since γ in general is inversely proportional to the fundamental band gap of semiconductors, we assume that γ_b ranges from 11 to 23 meV \AA^3 , with 11 meV \AA^3 a value roughly in GaAs and 23 meV \AA^3 the value of γ_w that we consider.
- [53] This matching boundary condition for the first derivative of wave function is a direct outcome of the Ben Daniel–Duke model [17,41].
- [54] Depending on the interplay of the quantities γ_w , γ_b , and $\psi_1'(z)$, β_{int} may even have a sign reversal in other parameter ranges.
- [55] L. Dekar, L. Chetouani, and T. F. Hammann, Wave function for smooth potential and mass step, *Phys. Rev. A* **59**, 107 (1999).
- [56] J. Schliemann, J. C. Egues, and D. Loss, Nonballistic Spin-Field-Effect Transistor, *Phys. Rev. Lett.* **90**, 146801 (2003).
- [57] B. A. Bernevig, J. Orenstein, and S.-C. Zhang, Exact SU(2) Symmetry and Persistent Spin Helix in a Spin-Orbit Coupled System, *Phys. Rev. Lett.* **97**, 236601 (2006).
- [58] J. D. Koralek, C. P. Weber, J. Orenstein, B. A. Bernevig, S.-C. Zhang, S. Mack, and D. D. Awschalom, Emergence of the persistent spin helix in semiconductor quantum wells, *Nature (London)* **458**, 610 (2009).
- [59] M. P. Walser, C. Reichl, W. Wegscheider, and G. Salis, Direct mapping of the formation of a persistent spin helix, *Nat. Phys.* **8**, 757 (2012).
- [60] R. Vaxenburg and E. Lifshitz, Alloy and heterostructure architectures as promising tools for controlling electronic properties of semiconductor quantum dots, *Phys. Rev. B* **85**, 075304 (2012).
- [61] A. Sashchiuk, D. Yanover, A. Rubin-Brusilovski, G. I. Maikov, R. K. Capek, R. Vaxenburg, J. Tilchin, G. Zaiats, and E. Lifshitz, Tuning of electronic properties in IV–VI colloidal nanostructures by alloy composition and architecture, *Nanoscale* **5**, 7724 (2013).
- [62] Y. J. Jang, A. Shapiro, M. Isarov, A. Rubin-Brusilovski, A. Safran, A. K. Budniak, F. Horani, J. Dehnel, A. Sashchiuk, and E. Lifshitz, Interface control of electronic and optical properties in IV–VI and II–VI core/shell colloidal quantum dots: A review, *Chem. Commun.* **53**, 1002 (2017).
- [63] X. Q. Hou, Y. Li, H. Y. Qin, and X. G. Peng, Effects of interface-potential smoothness and wavefunction delocalization on Auger recombination in colloidal CdSe-based core/shell quantum dots, *J. Chem. Phys.* **151**, 234703 (2019).
- [64] H. Sari, E. Kasapoglu, S. Sakiroglu, I. Sökmen, and C. A. Duque, Effect of intense laser field in Gaussian quantum well with position-dependent effective mass, *Phys. Status Solidi* **256**, 1800758 (2019).
- [65] M. P. Walser, U. Siegenthaler, V. Lechner, D. Schuh, S. D. Ganichev, W. Wegscheider, and G. Salis, Dependence of the Dresselhaus spin-orbit interaction on the quantum well width, *Phys. Rev. B* **86**, 195309 (2012).
- [66] J. Ishihara, Y. Ohno, and H. Ohno, Direct imaging of gate-controlled persistent spin helix state in a modulation-doped GaAs/AlGaAs quantum well, *Appl. Phys. Express* **7**, 013001 (2013).
- [67] In the parameter range considered, because the single heterostructure is much more asymmetric (as compared to the DH case), the Rashba strength in the SH configuration is far greater than the Dresselhaus strength, and thus the two terms are not matched (not shown).
- [68] M. M. Glazov, E. Y. Sherman, and V. K. Dugaev, Two-dimensional electron gas with spin-orbit coupling disorder, *Physica E* **42**, 2157 (2010).
- [69] E. Y. Sherman, Random spin-orbit coupling and spin relaxation in symmetric quantum wells, *Appl. Phys. Lett.* **82**, 209 (2003).
- [70] M. M. Glazov and E. Y. Sherman, Nonexponential spin relaxation in magnetic fields in quantum wells with random spin-orbit coupling, *Phys. Rev. B* **71**, 241312(R) (2005).
- [71] J. R. Bindel, M. Pezzotta, J. Ulrich, M. Liebmann, E. Y. Sherman, and M. Morgenstern, Probing variations of the Rashba spin-orbit coupling at the nanometre scale, *Nat. Phys.* **12**, 920 (2016).
- [72] J. Nitta, Ready for a close-up, *Nat. Phys.* **12**, 898 (2016).
- [73] E. I. Rashba and E. Y. Sherman, Spin-orbit band splitting in symmetric quantum wells, *Phys. Lett. A* **129**, 175 (1988).
- [74] M. V. Durnev, M. M. Glazov, and E. L. Ivchenko, Spin-orbit splitting of valence subbands in semiconductor nanostructures, *Phys. Rev. B* **89**, 075430 (2014).
- [75] J. W. Luo, A. N. Chantis, M. van Schilfgaarde, G. Bester, and A. Zunger, Discovery of a Novel Linear-in- k Spin Splitting for Holes in the 2D GaAs/AlAs System, *Phys. Rev. Lett.* **104**, 066405 (2010).
- [76] I. Jo, K. A. Villegas Rosales, M. A. Mueed, L. N. Pfeiffer, K. W. West, K. W. Baldwin, R. Winkler, M. Padmanabhan, and M. Shayegan, Transference of Fermi Contour Anisotropy to Composite Fermions, *Phys. Rev. Lett.* **119**, 016402 (2017).
- [77] J. Shabani, M. Shayegan, and R. Winkler, Strain-Induced Fermi Contour Anisotropy of GaAs 2D Holes, *Phys. Rev. Lett.* **100**, 096803 (2008).
- [78] A. A. High, A. T. Hammack, J. R. Leonard, S. Yang, L. V. Butov, T. Ostatnický, M. Vladimirova, A. V. Kavokin, T. C. H. Liew, K. L. Campman, and A. C. Gossard, Spin Currents in a Coherent Exciton Gas, *Phys. Rev. Lett.* **110**, 246403 (2013).
- [79] D. V. Vishnevsky, H. Flayac, A. V. Nalitov, D. D. Solnyshkov, N. A. Gippius, and G. Malpuech, Skyrmion Formation and Optical Spin-Hall Effect in an Expanding Coherent Cloud of Indirect Excitons, *Phys. Rev. Lett.* **110**, 246404 (2013).
- [80] S. V. Iordanskii, Y. B. Lyanda-Geller, and G. E. Pikus, Weak localization in quantum wells with spin-orbit interaction, *JETP Lett.* **60**, 206 (1994).